

tend to appear cumbersome and inconvenient for practical applications. In practice, however, only the first few terms in the summations will be significant. The number of these terms will clearly vary with the distance and temperature range under consideration and also with the convergence pattern of the coefficients in the series.

(5) The results of the present investigation give a

more comprehensive and unified picture of some aspects of the charge-screening problem in an electron gas than has yet been presented. They should be extremely useful in a wide range of problems, particularly those where elementary asymptotic field, such as the Friedel wiggle, are being employed. They should also serve as a useful first approximation in more sophisticated treatments of long-range charge screening in an electron gas.

PHYSICAL REVIEW

VOLUME 185, NUMBER 3

15 SEPTEMBER 1969

Specific Heat of *n*- and *p*-Type Bi₂Te₃ from 1.4 to 90°K*

G. E. SHOEMAKE† AND J. A. RAYNE

Carnegie-Mellon University, Pittsburgh, Pennsylvania 15213

AND

R. W. URE, JR.‡

Westinghouse Research Laboratories, Pittsburgh, Pennsylvania 15235

(Received 4 March 1969)

The specific heats of *n*-type bismuth telluride with carrier concentrations ranging between 2.2×10^{18} and 8.3×10^{20} cm⁻³, *p*-type Bi₂Te₃ with a carrier concentration of 1.3×10^{19} cm⁻³, and bismuth selenide have been measured from 1.3 to 90°K. At low temperatures, there are measurable differences in the electronic specific heat of *n*-type Bi₂Te₃ as a function of carrier concentration. These differences can be explained on the basis of a conduction band consisting of six ellipsoidal minima and an additional heavy-mass band lying approximately 30 meV above them. The electronic specific heat of *p*-type Bi₂Te₃ is consistent with a six-ellipsoid model. For both *n*- and *p*-type Bi₂Te₃, as well as Bi₂Se₃, departure of the lattice specific heat from the Debye T³ approximation begins well below the lowest temperatures measured. The extrapolated Debye temperature at absolute zero is (162 ± 3) °K for Bi₂Te₃, which agrees well with the value of (165 ± 2) °K obtained from the low-temperature elastic constants. Bi₂Se₃ has been found to have a limiting Debye temperature of (182 ± 3) °K.

I. INTRODUCTION

WITHIN the last ten years, a significant amount of progress has been made towards an understanding of the transport properties of Bi₂Te₃ in terms of an ellipsoidal multivalley model for its conduction and valence bands.^{1,2} Recent de Haas-van Alphen studies,^{3,4} together with related transport measurements on *n*-type Bi₂Te₃,⁵ have led to the postulates of an

additional heavy-mass low-mobility conduction band lying at a slightly higher energy than the ellipsoidal minima. The existence of such a band can be checked directly by examining the behavior of the electronic specific heat. Although specific-heat measurements have been made previously on Bi₂Te₃, none have been obtained for *n*-type material and indeed the electronic specific heat of *p*-type Bi₂Te₃ appears to be in serious disagreement with that calculated from the results of de Haas-van Alphen (dHvA) measurements. This work then is primarily concerned with an experimental determination of the specific heat of *n*-type Bi₂Te₃ to deduce information concerning the second band, and with a remeasurement of the electronic heat capacity of *p*-type material. Of interest, too, is the limiting Debye temperature Θ_0 , which can be compared with Θ_0 calculated from elastic constants, and the variation of the lattice heat capacity with temperature and doping impurities. The specific heat of bismuth selenide has also been measured to observe the difference in lattice heat capacity caused by the substitution of selenium for tellurium.

* Work supported by the Air Force Office of Scientific Research, Office of Aerospace Research, U. S. Air Force Grant No. AF-AFOSR-870-65. This paper is based on a thesis submitted by one of us (GES) as partial fulfillment of the requirements for the Ph.D. degree in Physics at Carnegie-Mellon University.

† Present address: General Dynamics, Fort Worth, Tex.

‡ Present address: College of Engineering, University of Utah, Salt Lake City, Utah, 84112.

¹ J. R. Drabble, in *Progress in Semiconductors*, edited by A. E. Gibson and R. E. Burgess (Wiley-Interscience, Inc., New York, 1963), Vol. 7, p. 47.

² H. J. Goldsmid, *J. Appl. Phys. Suppl.* **32**, 2198 (1961).

³ R. B. Mallinson, J. A. Rayne, and R. W. Ure, Jr., *Phys. Letters* **24A**, 713 (1967).

⁴ R. B. Mallinson, J. A. Rayne, and R. W. Ure, Jr., *Phys. Rev.* **175**, 1049 (1968).

⁵ R. W. Ure, Jr., in *International Conference on the Physics of Semiconductors, Exeter, 1962* (Institute of Physics and Physical Society, London, 1962), p. 659; Y. Yates, *J. Electronics Control*

6, 26 (1959); P. A. Walker, *Proc. Phys. Soc. (London)* **76**, 113 (1960).

II. THEORY

A. Electronic Specific Heat

The electronic heat capacity of a degenerate electron gas is given by the expression

$$C_{el} = \gamma T = \frac{1}{3} \pi^2 k_B^2 g_e(E_F) T, \quad (1)$$

where $g_e(E_F)$ is the density of states at the Fermi level. Substitution of the value of $g_e(E_F)$ for a spherical, parabolic band gives

$$C_{el} = \frac{\pi k_B^2 (3/\pi)^{1/3} m_0 A m^*}{3 \hbar^2 \rho m_0} n^{1/3} T. \quad (2)$$

In the latter equation, n is the number of carriers per cm^3 , A the atomic weight, ρ the mass density, m_0 the free-electron mass, and m^* the carrier effective mass. In units of $\text{mJ mole}^{-1} \text{deg}^{-2}$, the coefficient γ can be written as

$$\gamma = (1.609 \times 10^{-9}) (A/\rho) (m^*/m_0) n^{1/3}. \quad (3)$$

The band structure of many semiconductors is best described by a multivalley model having equivalent conduction-band minima, symmetrically arranged in the Brillouin zone such that they can be transformed one into another under the symmetry operations of the crystal. For ellipsoidal minima, the band energy referred to a valley minimum can be expanded in terms of the wave vector \mathbf{k} , also referred to the minimum, as

$$E(\mathbf{k}) = (\hbar^2/2m_0) (\alpha_{11}k_1^2 + \alpha_{22}k_2^2 + \alpha_{33}k_3^2 + 2\alpha_{12}k_1k_2 + 2\alpha_{23}k_2k_3 + 2\alpha_{31}k_3k_1), \quad (4)$$

where the components of \mathbf{k} refer to the crystal axes and the α_{ij} represent components of the inverse effective-mass tensor. Each of these ellipsoids contributes equally to the heat capacity according to Eq. (3), so that if n_i is written for the carrier concentration per ellipsoid and s for the number of ellipsoids, then the specific heat per ellipsoid is

$$C_{el}/s = (1.609 \times 10^{-9}) (A/\rho) (m^*/m_0) n_i^{1/3} T, \quad (5)$$

with the effective-mass ratio taken as

$$m^*/m_0 = (\det|\alpha|)^{-1/3}. \quad (6)$$

Since the ellipsoids are equivalent, the carrier concentration per ellipsoid is $n_i = n/s$ and hence the total molar electronic heat capacity becomes

$$C_{el} = (1.609 \times 10^{-9}) (A/\rho) (m^*/m_0) s^{2/3} n^{1/3} T \quad (7)$$

in units of $\text{mJ mole}^{-1} \text{deg}^{-1}$.

Assuming no nuclear contribution, the total heat capacity near absolute zero, where the Debye approximation holds, is given by

$$C_v = \gamma T + \beta (T/\Theta_0)^3. \quad (8)$$

The values of γ and Θ_0 can be obtained in the usual way by a least-squares fit of a straight line to experimentally

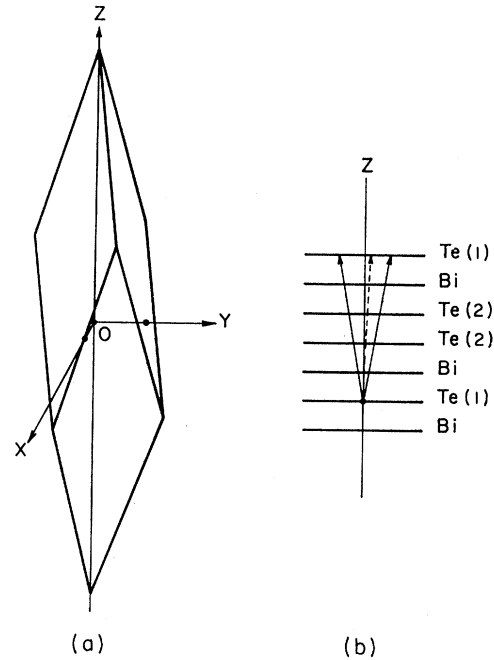


FIG. 1. (a) Schematic representation of the rhombohedral unit cell for Bi_2Te_3 showing the binary, bisectrix and trigonal axes OX , OY , and OZ ; (b) arrangement of atoms within the unit cell.

determined values of C/T versus T^2 at sufficiently low temperature. Clearly, γ is the intercept at $T=0$ and β/Θ_0^3 is the slope of this line.

B. Symmetry and Chemical Bonding

Bi_2Te_3 has a rhombohedral unit cell (space group $R\bar{3}m$) with a single threefold (trigonal) rotation axis, a center of symmetry and, in addition, three twofold axes normal to three reflection planes containing the trigonal axis. The unit cell is shown in Fig. 1(a), where Z is the trigonal axis. The atoms are arranged in layers perpendicular to the trigonal axis with each layer containing atoms of one kind only. The order of the layers is shown in Fig. 1(b). The indexing of the tellurium atom distinguishes between the two possible arrangements of neighboring atoms. It has been proposed⁶ that within each quintet unit shown in brackets —Bi—Te(2)—[Te(2)—Bi—Te(1)—Bi—Te(2)]—Te(2)—, valence forces bind the atoms together; but the bonds between the quintets are essentially due to weak van der Waals forces, which explains the layerlike cleavage characteristic for Bi_2Te_3 . Departure from the Debye T^3 behavior could occur in this situation with a possible^{7,8} T^2 dependence, associated with an effective two-dimensional lattice, appearing at moderately low temperatures.

⁶ J. R. Drabble and C. H. L. Goodman, *J. Chem. Phys. Solids* **5**, 142 (1958).

⁷ E. S. Itskevich and P. G. Strelkov, *Zh. Eksperim. i Teor. Fiz.* **32**, 467 (1957) [English transl.: *Soviet Phys.—JETP* **5**, 394 (1957)].

⁸ I. M. Lifshitz, *Zh. Eksperim. i Teor. Fiz.* **22**, 471, 475 (1952).

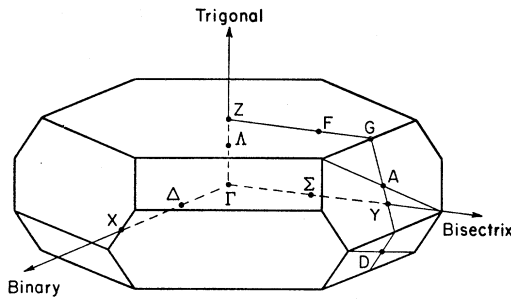


FIG. 2. Brillouin zone for Bi_2Te_3 showing the location of the symmetry points. The scale of the drawing has been exaggerated along ΓZ for purposes of clarity.

Figure 2 shows the Brillouin zone of Bi_2Te_3 ; clearly it is highly compressed in the direction parallel to the trigonal axis because of the large c/a ratio. This compression of the zone, as well as the highly anisotropic bonding, restricts the validity of the Debye approximation for the lattice specific heat to temperatures only a few tenths of a degree above absolute zero.

C. Band Structure (*n*-Type)

Experiments^{1,2} dealing with the transport properties of bismuth telluride and recent dHvA measurements^{3,4,9} have established the validity of a six-ellipsoid multi-valley conduction-band model for *n*-type Bi_2Te_3 at low carrier concentrations. Two axes of each ellipsoid lie in the mirror planes. With this position of the valleys, two of the off-diagonal terms α_{ij} of Eq. (4) must be zero and the conduction-band energy referred to the valley minimum for a representative ellipsoid is

$$E(\mathbf{k}) = (\hbar^2/2m_0)(\alpha_{11}k_1^2 + \alpha_{22}k_2^2 + \alpha_{33}k_3^2 + 2\alpha_{23}k_2k_3), \quad (9)$$

where the indices 1, 2, and 3 represent the binary, bisectrix, and trigonal axes, respectively. The ellipsoids are thought to lie near the points *D* in the Brillouin zone. Recent pseudopotential calculations¹⁰ tend to confirm this assignment. Table I shows the experimental values of α_{ij} obtained from dHvA data. For *n*-type Bi_2Te_3 , these parameters are essentially independent of carrier concentration in the range 9×10^{17} – $2.4 \times 10^{19} \text{ cm}^{-3}$. The corresponding value of average effective mass calculated from Eq. (6) is $m^* = 0.101m_0$.

The carrier density n_E in the conduction band, as measured by the dHvA effect, can be computed from the ellipsoid volume given by Eq. (9) assuming that there are six minima. Its variation with the total number of carriers n_H is shown in Fig. 3. Here n_H is determined from the two independent Hall coefficients ρ_{123} and ρ_{321} . These coefficients should saturate to the same value in the high-field limit, where $\omega\tau \gg 1$, $\omega = eH/m^*c$ being the cyclotron frequency and τ the

⁹ R. B. Mallinson, J. A. Rayne, and R. W. Ure, Jr., Phys. Letters **19**, 545 (1965).

¹⁰ F. Borghese and E. Donato, Nuovo Cimento **53**, 283 (1968).

TABLE I. Mass parameters for the representative ellipsoid of Bi_2Te_3 and the average effective mass m^* .

Carrier type	α_{11}	α_{22}	α_{33}	α_{23}	m^*/m_0
<i>n</i> type ^a	34.6	4.35	6.86	1.53	0.101
<i>p</i> type ^b	20.8	2.80	4.65	-1.05	0.159

^a See Ref. 4.

^b See Ref. 11.

scattering time. As can be seen in Fig. 4, this behavior was observed in some samples. In other cases, however, the convergence is not complete, owing presumably to specimen inhomogeneity. For this case, an average of the two coefficients at high magnetic field is taken. The limiting Hall constant R_H and the carrier concentration are related by

$$n_H = 1/R_H e. \quad (10)$$

From Fig. 3, it can be seen that for low carrier densities the experimental points lie on the straight line corresponding to $n_H = n_E$. However, for carrier concentrations exceeding $n_H = 4.4 \times 10^{18} \text{ cm}^{-3}$, n_E begins to fall below the total number of carriers, the difference between n_E and n_H becoming quite pronounced as n_H continues to increase. To explain these data, it has been proposed^{3,4} that a second band with high effective mass and low mobility must be located approximately 30 meV above the conduction-band minima of the first band. As the total number of carriers n_H exceeds some fixed carrier concentration n_x determined by ΔE (the energy separation between the bottom of the ellipsoid valleys of the first band and the bottom of the second band), electrons also begin to fill this second band and the Fermi energy, and hence n_E , increases more slowly as a function of n_H . The low mobility and high effective mass of these second band electrons are such that these

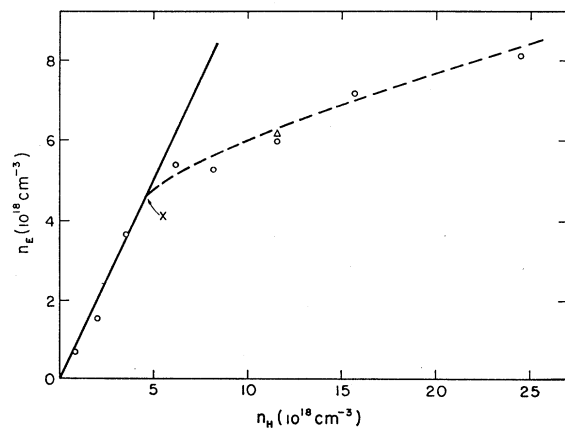


FIG. 3. Dependence of n_E , the carrier density derived from dHvA data, on n_H the carrier concentration determined from the limiting high-field Hall coefficient at 4.2°K. The full line is the relation $n_E = n_H$, while the dashed curve is a least-squares fit to the data for high carrier density assuming a parabolic second band.

TABLE II. The average carrier concentration n_{av} and the variation of n along the length of the parent ingot for each specific-heat sample. The value of n is obtained from R measured at 77°K and 6 kG with H perpendicular to the cleavage plane.

Sample	Type of doping	Subspecimen carrier density n (cm^{-3})	n_1 (average) (cm^{-3})	n_{av} (cm^{-3})
1	<i>n</i> -type iodine	1.7×10^{18} 3.6	2.7×10^{18}	$2.2 \pm 0.5 \times 10^{18}$ ^a
2	<i>n</i> -type iodine	1.84×10^{19} 2.76 3.00 3.03	2.7×10^{19}	$1.6 \pm 0.4 \times 10^{18}$ ^a
3	<i>n</i> -type tellurium	13.6×10^{19} 7.30 4.77 6.32 1.84	6.8×10^{19}	$3.9 \pm 2 \times 10^{19}$
4	<i>n</i> -type iodine	6.8×10^{20} ^b 8.4 9.3 8.7	8.3×10^{20} ^b	$8 \pm 3 \times 10^{20}$ ^b
5	<i>p</i> -type	1.68×10^{19} 1.76 1.98 2.44	2.0×10^{19}	$1.3 \pm 0.2 \times 10^{19}$ ^a

^a Computed from n_1 (average) and Fig. 5.
^b Measured only at room temperature.

carriers can contribute to the measured Hall voltage and yet apparently produce no observable dHvA signal below 30 kG. This signal, whose amplitude is proportional to a damping factor $\exp[-2\pi^2 k_B m^* c(T+T^*)/ehH]$ with T^* associated with the broadening of the Landau levels, should be detectable, however, at much higher magnetic fields.

The second band parameters m_2^* , ΔE , and n_x together with the shape of the dashed curve in Fig. 3 have been calculated by a least-squares fit of the dHvA experi-

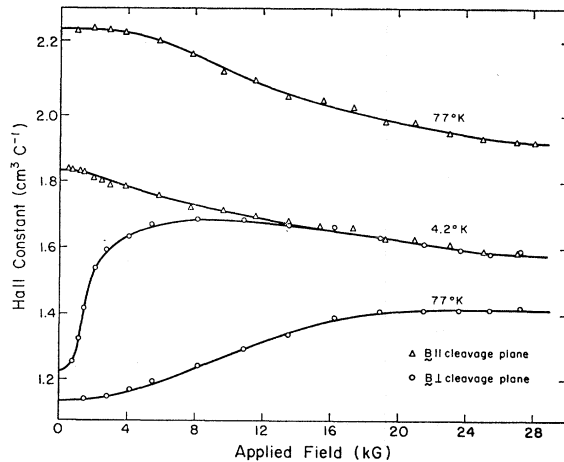


Fig. 4. Typical Hall data for *n*-type Bi_2Te_3 showing the variation of ρ_{123} and ρ_{312} with field at both nitrogen and helium temperatures. The carrier concentration obtained from the limiting high-field Hall constant at 4.2°K is $3.7 \times 10^{18} \text{ cm}^{-3}$.

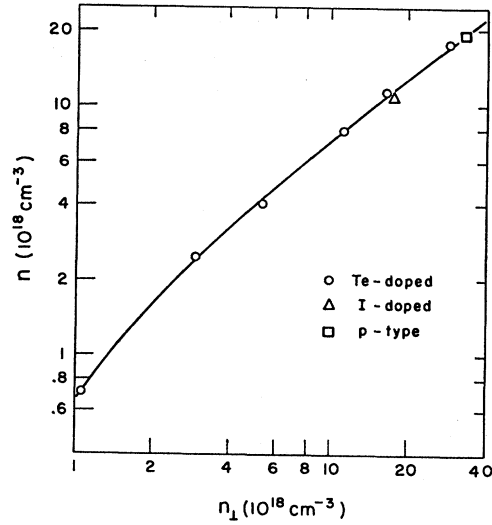


Fig. 5. Variation of n_H measured at 4.2°K and 28 kG with the value of n_1 , the carrier density measured at 77°K with a perpendicular field of 6 kG.

mental data above $n_H = 4 \times 10^{18}$ to an expression of the form

$$(n_H - n_E)^{2/3} = b n_E^{2/3} - a. \quad (11)$$

This relation is derived on the assumption of a parabolic second band with the constants a and b related to the above parameters by

$$b = (m_2^*/m_1^* s^{2/3}), \quad a = [(m_2^*/m_0)/K_0] \Delta E, \quad (12)$$

$$n_x = (a/b)^{3/2},$$

where $K_0 = (\frac{3}{8}\pi^{1/2})^{2/3} (h^2/2\pi m_0)$. With $m_1^* = 0.101 m_0$, $s = 6$ for the first band, and $K_0 = 3.62 \times 10^{-12} \text{ meV cm}^2$, the parameters of the second band are found from Eqs. (11) and (12) to be $m_2^* = 1.49 m_0$, $\Delta E = 29.3 \text{ meV}$, and $n_x = 4.4 \times 10^{18} \text{ cm}^{-3}$.

D. Band Structure (*p*-Type)

A six-ellipsoid model has been found to fit the dHvA data¹¹ for *p*-type Bi_2Te_3 , the general shape of the representative ellipsoid being the same as for *n*-type material. The relevant effective-mass parameters α_{ij} , which are listed in Table I, give an effective mass $m^* = 0.16 m_0$. There is considerable disagreement between this value and an effective mass of $m^* = 0.47 m_0$ computed from earlier¹² electronic specific-heat measurements. No indication of a second band has been found.

III. EXPERIMENT

A. Samples

All samples have been prepared from 99.999% pure starting materials using a horizontal loaded-zone

¹¹ L. R. Testardi, P. J. Stiles, and E. Burstein, *Solid State Commun.* **1**, 28 (1963).

¹² E. S. Itskevich, *Zh. Eksperim. i Teor. Fiz.* **38**, 351 (1960) [English transl.: *Soviet Phys.—JETP* **11**, 255 (1960)].

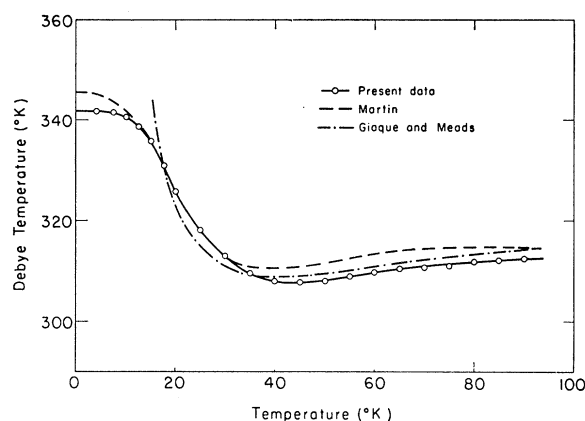


FIG. 6. Variation with temperature of the Debye Θ for copper as obtained in this work and in previous experiments.

technique. In this technique, a molten zone whose composition is different from the composition of the solid is passed along the length of a solid bar. The ingots were 10 in. long with a cross section that is roughly a half circle of $\frac{5}{8}$ in. diam. The ingots were polycrystalline with three to six crystals running along the length. The individual grains were large enough that single-crystal Hall samples could be cut from the ingots.

One Bi_2Te_3 crystal (sample No. 5) was grown from a stoichiometric melt; as expected, it is p type. n -type material can be made by doping the molten zone with either a foreign impurity such as iodine or with excess tellurium. Iodine-doped crystals are heavily compensated, so tellurium-doped crystals are used for measurements, such as the dHvA effect, which require high mobility at low temperatures. However, it is difficult to grow ingots with uniform carrier concentration from excess tellurium melts. The reason for this is that the melt must contain 63–65 at. % tellurium in order to obtain n -type material. The carrier concentration in the solid increases with an increasing excess of tellurium in the melt. Since the solid on both sides of the molten zone has a composition very close to 60 at. % tellurium, the composition of the melt and therefore the carrier concentration in the growing crystal changes with unavoidable changes in the length of the molten zone. In the case of crystals grown from iodine-doped melts, the iodine concentrations in the liquid and the melt are more nearly equal so the melt composition does not change as rapidly with changes in the length of the molten zone. Three n -type crystals were made with iodine doping, and one was grown from an excess tellurium melt to check whether there were any differences.

Each ingot was cut into three or four 2-in. pieces which were used for the specific-heat measurements. Smaller samples for Hall-effect measurements were cut between the larger pieces in order to determine the carrier concentration and homogeneity. Hall data, giving R_L and hence n_L , with the magnetic field perpen-

dicular to the cleavage plane have been taken on these samples at 77°K in a magnetic field intensity of 6 kG. For n_L less than $4.0 \times 10^{19} \text{ cm}^{-3}$, the average carrier concentration is calculated using the smooth curve of Fig. 5. This curve has been obtained from an independent series of experiments, taken both at liquid-nitrogen and liquid-helium temperatures, as a function of magnetic field. The carrier density n for sample No. 3 lies beyond the limits of the curve and has been calculated as the average of n_L and n_{11} (magnetic field parallel to the cleavage plane) measured at 11 kG and 77°K. Sample No. 4 has only been measured at room temperature. A summary of the carrier concentrations for each of the samples is given in Table II.

B. Apparatus

A standard calorimeter, based on a design by Manchester¹³ incorporating a mechanical heat switch, has been used in this work. Temperatures are measured with a calibrated, CryoCal Inc. four-terminal, encapsulated germanium resistor. This unit is contained, together with the heater, in a copper-beryllium housing which clamps on to the sample holder. The temperature range between 1.2 and 28°K is divided into three separate calibration regions. In each region the resistance-versus-temperature relation is fitted to an expression of the form

$$\log T_R = a + b \log R + c (\log R)^2, \quad (13)$$

so as to produce deviation plots of $(T - T_R)$ versus T_R . For the lowest range between 1.2 and 4.2°K, the thermometer has been calibrated against the 1958 He^4 vapor pressure scale with an error of less than 0.0005°K. For temperatures between 4.2 and 28°K, the calibration is traceable to a gas thermometer with an estimated error of less than 0.001–0.005°K. Between 28 and 100°K, the thermometer has been calibrated against an NBS platinum resistance standard to generate a table of resistance versus temperature spaced approximately every 0.5°K. A Legendre polynomial interpolation scheme using this table is then employed to find actual temperatures.

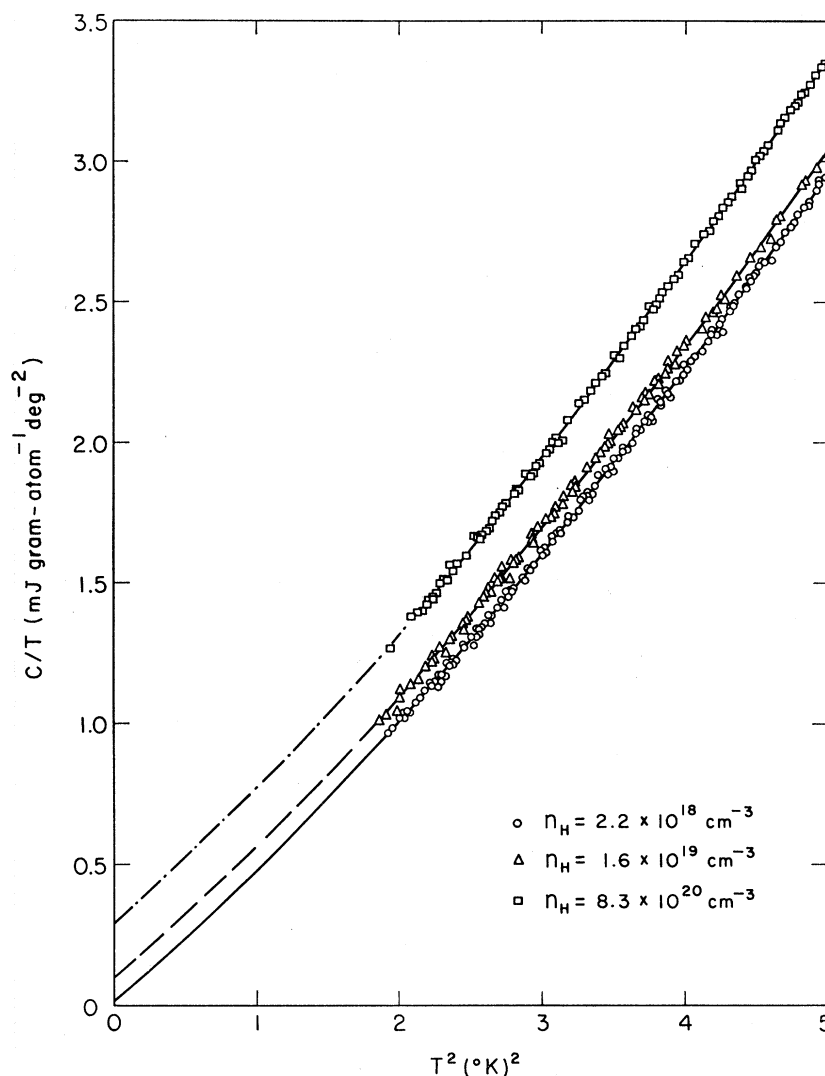
IV. RESULTS

A. Copper

To check the performance of the calorimeter, a specimen of high-purity copper has been measured over the entire temperature range of interest. This sample, weighing 135.4 g, has been prepared by vacuum fusion of 99.999+ % pure copper obtained from the American Smelting and Refining Company. A least-squares fit of the data below 4.2°K gives values of $\gamma = 0.700 \pm 0.006 \text{ mJ mole}^{-1} \text{ deg}^{-2}$ and $\Theta_0 = 342 \pm 3^\circ\text{K}$, which compare favorably with those obtained by other

¹³ F. D. Manchester, Can. J. Phys. 37, 989 (1959).

FIG. 7. Plot of C/T versus T^2 for n -type iodine-doped Bi_2Te_3 with varying carrier concentrations. The full line is a polynomial fit to the data for the lowest carrier concentration, constrained to pass through the computed value of γ_{ref} at $T^2=0$. The dashed lines are fits to the data for higher carrier densities assuming the same lattice heat capacity as for the reference sample.



workers.¹⁴ The quoted uncertainties represent random errors plus systematic errors estimated to be approximately 0.5%. Good agreement with previous work^{15,16} for temperatures above 4°K has also been obtained, as shown in the plot of Θ versus T in Fig. 6.

B. Addendum

The addendum consists of the aluminum sample holder and copper-beryllium clamp containing the heater and thermometer. Its heat capacity, C_{add} , has been measured to 1% accuracy below 4.2°K and a table of C_{add} versus temperature constructed for interpolation. Although kept as small as possible, the addendum contributes in some cases as much as 40%

¹⁴ D. W. Osborne, H. E. Flotow, and J. Schreiner, *Rev. Sci. Instr.* **38**, 159 (1967).

¹⁵ D. L. Martin, *Phys. Rev.* **141**, 141 (1966).

¹⁶ W. F. Giaque and P. F. Meads, *J. Am. Chem. Soc.* **63**, 1897 (1941).

to the total heat capacity below 1.5°K for a Bi_2Te_3 sample, dropping off to 20% at 2.5°K and 10% at 4.2°K. An uncertainty of 1% in C_{add} , therefore, gives as much as 0.7% uncertainty in the specific heat of Bi_2Te_3 at the lowest temperatures.

C. Bismuth Telluride

Five different samples of Bi_2Te_3 have been measured between 1.35 and 4.2°K, the results of these measurements at the lowest temperatures being shown in Figs. 7-9. Figure 10 gives the variation of Θ with temperature for the sample with the lowest carrier density. This curve represents the lattice specific heat of Bi_2Te_3 , in general, provided the impurity dopants do not alter appreciably the characteristics of the lattice, as seems reasonable. The type and number of carriers of each sample has been given previously in Table II.

Lattice specific heat. At the lowest temperatures measured, there is obvious departure from a straight

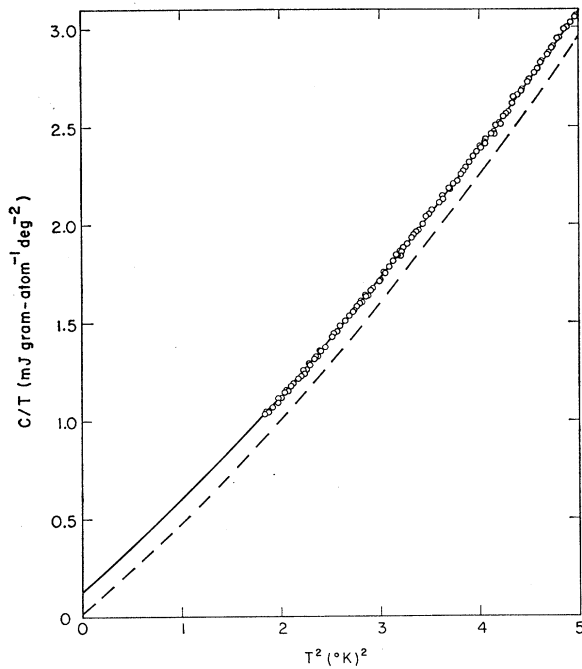


FIG. 8. Plot of C/T versus T^2 for n -type tellurium-doped Bi_2Te_3 with a carrier concentration of $3.9 \times 10^{19} \text{ cm}^{-3}$. The dashed line is the corresponding plot for the reference sample.

line predicted by Eq. (8) for the C/T -versus- T^2 plots given in Figs. 7-9. Because the lattice heat capacity deviates significantly from T^3 behavior even above

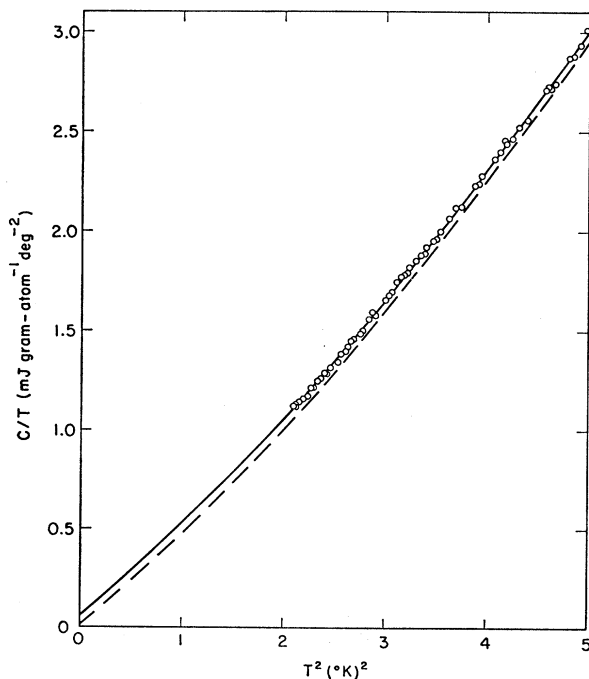


FIG. 9. Plot of C/T versus T^2 for stoichiometric p -type Bi_2Te_3 with a carrier concentration of $3.5 \times 10^{19} \text{ cm}^{-3}$. The dashed line is the corresponding plot for the reference sample.

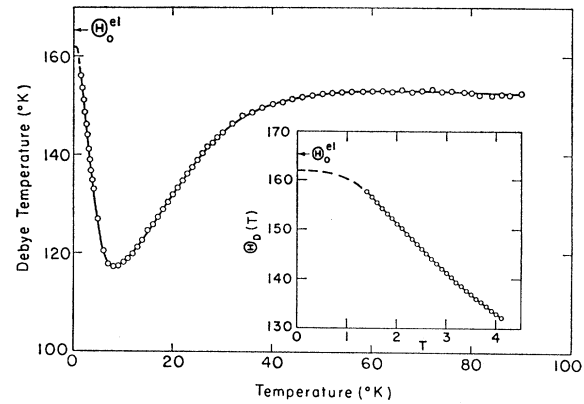


FIG. 10. Temperature variation of Debye Θ for Bi_2Te_3 . The inset shows the behavior near absolute zero and the corresponding value of Θ_0^{el} obtained from elastic data.

1.3°K , it is not possible to obtain accurate values of Θ_0 and γ from a least-squares-fitting procedure, owing to the large T^5 term. The limiting Debye temperature Θ_0 can be computed, however, from the slope of the extrapolated linear region of the curve for the sample with the lowest carrier concentration. Since the six-ellipsoid model is valid in this case, the intercept at $T^2=0$ can be calculated from Eq. (7) using the appropriate carrier concentration and effective mass. This procedure gives a value $\Theta_0=162 \pm 2^\circ\text{K}$, the errors arising primarily from estimating the behavior of the curve near absolute zero. This compares very well with the value $\Theta_0^{\text{el}}=165 \pm 2^\circ\text{K}$ obtained from the elastic constants¹⁷ of Bi_2Te_3 extrapolated to absolute zero.

Two other specific-heat measurements at low temperatures have been published^{1,12} for bismuth telluride. It is interesting to note that both investigators claim a linear T^3 behavior below 2.3°K with Debye temperatures of 145°K and $155.5 \pm 3^\circ\text{K}$, respectively. These values are quite low compared with Θ_0^{el} and it appears that they are in error, perhaps due to an incorrect calculation of the specific heats of the addenda used in the experiments. It would indeed be surprising if the Debye theory were to hold for Bi_2Te_3 up to 2.3°K , considering the large elastic anisotropy and the shape of the Brillouin zone discussed previously. Bismuth,¹⁸ for example, with similar anisotropy exhibits obvious departure from a T^3 lattice specific heat even below 1°K . Arsenic and antimony¹⁹ also show noncubic lattice specific-heat behavior below 3°K , which is attributed to soft modes in the vibrational spectrum.

The lattice specific heats of samples 1, 2, and 5 have been measured up to 90°K and differ from one another by less than 1% over the entire temperature range, well within experimental scatter and error. Thus no measurable change in the lattice heat capacity is observed due

¹⁷ J. Jenkins (private communication).

¹⁸ N. E. Phillips, Phys. Rev. **118**, 644 (1960).

¹⁹ H. V. Culbert, Phys. Rev. **157**, 560 (1967).

TABLE III. $\Delta(C/T)$ for each sample of Bi_2Te_3 relative to sample of lowest carrier density. The values of $\Delta\gamma_{\text{val}_0}$ are computed from Eqs. (7), (14), and (16).

Sample	Carrier concentration (cm^{-3})	Number of bands	$\Delta\gamma$ ($\text{mJ g-at.}^{-1} \text{ deg}^{-2}$)		γ ($\text{mJ g-at.}^{-1} \text{ deg}^{-2}$)	
			Expt	Calc	Expt	Calc
1	2.17×10^{18} <i>n</i> type	one				0.014 ± 0.001
2	1.61×10^{19} <i>n</i> type	one two	0.085 ± 0.02	0.013 ± 0.02 0.108 ± 0.02	0.099 ± 0.02	0.027 ± 0.001 0.122 ± 0.02
3	3.9×10^{19} <i>n</i> type	one two	0.130 ± 0.02	0.023 ± 0.006 0.158 ± 0.03	0.144 ± 0.02	0.037 ± 0.005 0.172 ± 0.03
4	8.3×10^{20} <i>n</i> type	one two	0.30 ± 0.1	0.089 ± 0.015 0.42 ± 0.06	0.314 ± 0.1	0.103 ± 0.015 0.434 ± 0.06
5	1.27×10^{19} <i>p</i> type	one	0.052 ± 0.025		0.066 ± 0.025	0.040 ± 0.005
	3.5×10^{19} *	one			0.17 ± 0.08	0.055 ± 0.005

* See Ref. 12.

to doping. The lattice heat capacity has been calculated by subtracting the electronic term γT , insignificant above 3°K , from the total heat capacity corrected from constant pressure to constant volume using the Nernst-Lindeman relation $C_p - C_v = AC_p^2 T$. A is taken to be $3.54 \times 10^{-9} \text{ mJ g-at.}^{-1}$ and is computed at 100°K . The variation of Θ with T , shown in Fig. 10, is computed from the relation $C_{\text{lattice}} = f_D(T/\Theta)$, where $f_D(T/\Theta)$ is the usual Debye function of the reduced temperature T/Θ . There is reasonable agreement with the results of Itskovich¹² for *p*-type bismuth telluride.

Electronic specific heat. As pointed out earlier, there exist large uncertainties in the coefficient γ of the electronic heat capacity, when the data are fit by a least-squares method to an expression of the form $C/T = \gamma + \beta T^2 + \delta T^4$. However, as can be seen from Figs. 7-9, the curves of C/T versus T^2 for the samples are essentially parallel over the entire temperature range shown. The differences $\Delta(C/T)$ can therefore reasonably be attributed to the differences in γ associated with the number of carriers in each sample, since as has been noted previously the lattice heat capacity is not affected measurably by the type and degree of doping. Thus while the absolute values of γ cannot be measured accurately, the electronic behavior of the additional carriers in samples 2, 3, 4, and 5 compared to the reference sample No. 1 can be obtained from the equation

$$\Delta\gamma_i = \Delta(C/T)_i = (C/T)_i - (C/T)_{\text{ref}} = \gamma_i - \gamma_{\text{ref}}, \quad (14)$$

where the index i refers to samples 2, 3, 4, or 5 and C is the total heat capacity. The lattice heat capacities are essentially equal and hence their difference in Eq. (14) is zero.

To obtain $\Delta\gamma$ for each of the samples, the experimental specific-heat points of the reference sample in the temperature range up to $T^2 = 5$ have been fitted to a

T^5 polynomial to give the smooth curve of Fig. 7. The curve is adjusted so that it has an intercept at $T^2 = 0$ equal to the calculated value $\gamma_{\text{ref}} = 0.014 \text{ mJ g-at.}^{-1} \text{ deg}^{-2}$. From the individual experimental points of a given sample, corresponding values of $(C/T)_{\text{ref}}$ taken from this smooth curve have been subtracted and the differences subjected to a least-squares analysis based on an equation of the form, for the i th experimental point,

$$(C_i - C_{\text{ref}}) = \Delta C = \Delta\gamma_i T. \quad (15)$$

The curves drawn through the experimental points of samples 2, 3, and 5 are the results of this procedure with each curve having the same limiting slope and hence the same Debye temperature Θ_0 . The heat capacity of sample 4 cannot be fitted to the above expression for ΔC , since $\Delta(C/T)$ varies from 0.3 to $0.4 \text{ mJ g-at.}^{-1} \text{ deg}^{-2}$ between $T^2 = 2$ and $T^2 = 5$, owing probably to the large impurity concentration which significantly alters the lattice specific heat.

The resulting experimental values of $\Delta\gamma$ for *n*-type Bi_2Te_3 appear in Table III, together with predictions of $\Delta\gamma$ and γ based on both a single-band and a two-band model to be discussed in Sec. V. For sample No. 4 the value of $\Delta\gamma$ is taken at the lowest temperature measured; its limiting value at $T^2 = 0$ will certainly be less. Also given for completeness in Table III are $\Delta\gamma$ and γ for *p*-type Bi_2Te_3 . The limits of error associated with the experimental values of $\Delta\gamma$, except for sample 4 as discussed above, have been assigned on the basis of a 1% experimental error in the heat capacity of each sample at 1.5°K . This error is due primarily to the accuracy in the measurement of ΔT , the error introduced by the large contribution of the addenda being approximately the same for all samples and hence eliminated in $\Delta\gamma$. An additional $0.005 \text{ mJ g-at.}^{-1} \text{ deg}^{-2}$ error is included for the *p*-type sample, as a consequence of the greater scatter and fewer number of data points.

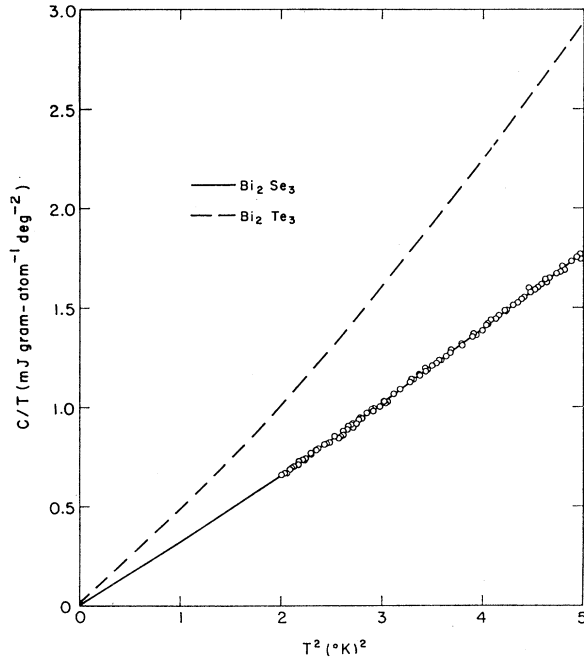


FIG. 11. Plot of C/T versus T^2 for Bi_2Se_3 with a carrier concentration of $2 \times 10^{19} \text{ cm}^{-3}$. The dashed line is the corresponding plot for the reference sample of Bi_2Te_3 .

D. Bismuth Selenide

A single stoichiometric sample of high-purity Bi_2Se_3 weighing 226.5 g, has been prepared in the same manner as Bi_2Te_3 , using 99.999% pure starting materials. Data for its low-temperature specific heat are given graphically in Fig. 11; its characteristic Debye temperature Θ between 0 and 90°K is shown in Fig. 12.

Clearly, the departure from T^3 behavior at the lowest temperatures measured, while not as pronounced as in the case of Bi_2Te_3 , does not allow an accurate computation of γ and Θ_0 using a curve-fitting technique. As before, the curve must be extrapolated to $T^2=0$ to obtain the limiting Debye temperature of $\Theta_0=182 \pm 3^\circ\text{K}$. The intercept at absolute zero indicates a very small electronic heat capacity of less than 0.01 mJ g-at. $^{-1}$ deg $^{-2}$, which agrees with a value of 0.006 mJ g-at. $^{-1}$ deg $^{-2}$ estimated from a single-ellipsoid model, for an effective mass²⁰ of $0.10m_0$ and the average carrier concentration of $2 \times 10^{19} \text{ cm}^{-3}$.

V. INTERPRETATION OF RESULTS

The single-band and two-band models for Bi_2Te_3 , as discussed previously, can be used to compute the electronic heat capacity and the difference in γ among the individual samples measured. These values $\Delta\gamma_{\text{calc}}$, when compared with the experimental values $\Delta\gamma_{\text{expt}}$

test the validity of each of the two models. The results are summarized in Table III.

A. Single-Band Model

The coefficient γ for each sample has been calculated, using Eq. (7), from the appropriate (n - or p -type) six-ellipsoid model with the effective mass given in Table I, the carrier concentration n_{av} taken from Table II, and the number of ellipsoids equal to six. The values γ_{calc} , associated with a single-band model, are given in Table III with the assigned error limits based on the accuracy of n_{av} for each sample. For the p -type sample a larger error is quoted, due to a somewhat less reliable effective mass calculated from the p -type mass parameters in Table I. With $\gamma_{\text{calc}}=0.014 \text{ mJ g-at.}^{-1} \text{ deg}^{-2}$ for the reference sample, Eq. (14) gives $\Delta\gamma_{\text{calc}}$ for each of the samples. For the n -type specimens, a comparison between $\Delta\gamma_{\text{calc}}$ and $\Delta\gamma_{\text{expt}}$ clearly shows a large disagreement with the single-band model, which accounts for less than 20% of the additional electronic heat capacity measured for samples 2 and 3.

B. Two-Band Model

This discrepancy is removed if the existence of the second band, described previously, is assumed. The electronic heat capacity becomes the sum of two terms of the form given by Eq. (7), one representing the first band contribution and the second the higher band contribution. Thus, the total electronic specific heat is

$$C_{e1} = K \left(\frac{m_1^*}{m_0} s_1^{2/3} n_1^{1/3} + \frac{m_2^*}{m_0} s_2^{2/3} n_2^{1/3} \right) T, \quad (16)$$

where m_1^* and m_2^* , s_1 and s_2 , and n_1 and n_2 represent the effective mass, number of ellipsoids, and carrier concentrations for the first and second bands, respectively. The carrier density n_1 is given by n_E in Fig. 3, while n_2 is just the difference between the total carrier density n_H and n_1 . As discussed earlier, the effective masses are, respectively, $m_1^*=0.101m_0$ and $m_2^*=1.49m_0$. The constant K is equal to 3.239×10^{-8} for C_{e1} expressed in units of mJ g-at. $^{-1}$ deg $^{-1}$. The values of γ_{calc} and $\Delta\gamma_{\text{calc}}$ calculated from Eq. (16), assuming that the carriers in the second band are contained in a single ellipsoid (i.e., $s_2=1$), are given in Table III. The limits of error are based on the accuracy of the average carrier concentration n_{av} , a 20% uncertainty in m_2^* ,

TABLE IV. Lattice parameters and molecular weights of Bi_2Te_3 and Bi_2Se_3 .

Material	Lattice parameter a_0 (Å)	Rhombohedral angle α	Molecular weight
Bi_2Te_3	10.473	$24^\circ 10'$	800.8
Bi_2Se_3	9.841	$24^\circ 16'$	654.8

²⁰ Calculated from the data of I. M. Tsidil'kovskii, *Thermomagnetic Effects in Semiconductors* (Infosearch, London, 1962).

and the accuracy of the curve in Fig. 3 above $n_H = 4 \times 10^{18} \text{ cm}^{-3}$ used to compute n_1 and n_2 . Within the combined errors, there is agreement between $\Delta\gamma_{\text{expt}}$ and $\Delta\gamma_{\text{calc}}$ for a two-band model. The fact that the experimental values of $\Delta\gamma$ for samples 2 and 3 are approximately $0.025 \text{ mJ g-at.}^{-1} \text{ deg}^{-2}$ below the values predicted by the two-band model is perhaps suggestive of a systematic error in the specific heat of the reference sample or a choice of m_2^* which is too high. The former is not likely since the data are reproducible and the same systematic errors appear in the heat-capacity measurements of each sample, thus tending to cancel when $\Delta\gamma$ is computed. Furthermore, $\Delta\gamma$ for the p -type material is found to be larger than its corresponding $\Delta\gamma_{\text{calc}}$ discussed below. The greatest uncertainty comes, most likely, in the determination of m_2^* from the least-squares-fitting procedure used for the determination of the dashed curve in Fig. 3. Indeed, if the second band were to begin filling at $n_H = 3.5 \times 10^{18} \text{ cm}^{-3}$, rather than at $4.4 \times 10^{18} \text{ cm}^{-3}$ (as is possible considering the scatter in the dHvA data of Fig. 3), the effective mass m_2^* would be lowered to $1.2m_0$ and $\Delta\gamma_{\text{calc}}$ would agree completely with $\Delta\gamma_{\text{expt}}$. It is also of interest to note that a difference in specific heat between samples 2 and 3, independent of sample 1, gives $\Delta\gamma$ of 0.010 and 0.050 $\text{mJ g-at.}^{-1} \text{ deg}^{-2}$ for a single-band and two-band calculation, respectively. This figure, when compared with the experimental value of $0.045 \text{ mJ g-at.}^{-1} \text{ deg}^{-2}$, gives more support for the existence of the second conduction band.

The specific heat of the high carrier density specimen, sample No. 4, also suggests a high mass second band even though a good comparison cannot be made with the other n -type samples because of the variation of $\Delta\gamma_{\text{expt}}$ with temperature due to the large degree of doping. The experimental value of $\Delta\gamma = 0.30 \pm 0.1 \text{ mJ g-at.}^{-1} \text{ deg}^{-2}$, at the lowest temperature measured, compares reasonably well with the second band result of $0.42 \pm 0.06 \text{ mJ g-at.}^{-1} \text{ deg}^{-2}$, which has been computed from an extrapolation of the curve in Fig. 3 to $n_H = 8.3 \times 10^{20} \text{ cm}^{-3}$. The substantial limits of error associated with the first band result of $\Delta\gamma = 0.089 \pm 0.015 \text{ mJ g-at.}^{-1} \text{ deg}^{-2}$, as well as the second band value, is due to the large uncertainty in the carrier concentration of sample 4. An additional error, from the extrapolation in Fig. 3, is also introduced in the second band calculation.

TABLE V. The high- and low-temperature limiting Debye temperature of Bi_2Te_3 and Bi_2Se_3 and the dependence of Θ_0/Θ_∞ on the mass ratio $(M_\infty/M_0)^{1/2}$.

Material	Θ_0 (°K)	Θ_∞ (°K)	Θ_0/Θ_∞	$(M_\infty/M_0)^{1/2}$	$(\Theta_0/\Theta_\infty)(M_\infty/M_0)^{-1/2}$
Bi_2Te_3	162	153	1.06	0.972	1.09
Bi_2Se_3	182	200	0.908	0.896	1.01

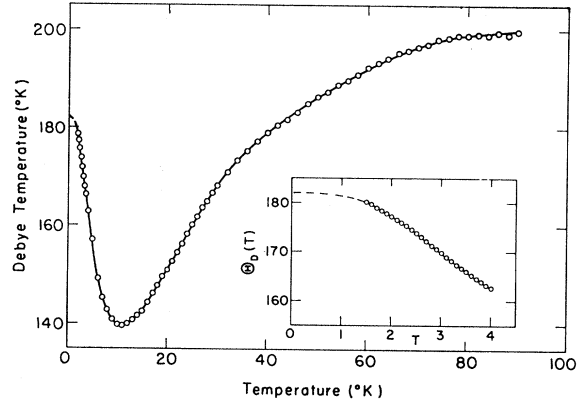


FIG. 12. Temperature variation of Θ for Bi_2Se_3 ; the inset shows the behavior near absolute zero.

C. p -Type Bi_2Te_3

A six-ellipsoid model using an effective mass $m^* = 0.159m_0$ for the p -type sample gives an electronic term $\gamma = 0.040 \pm 0.005 \text{ mJ g-at.}^{-1} \text{ deg}^{-2}$, which is in reasonable agreement with the experimental value of $0.066 \pm 0.025 \text{ mJ g-at.}^{-1} \text{ deg}^{-2}$ considering the large error limits of each value. In view of this agreement, the six-ellipsoid model for p -type bismuth telluride appears to be correct. One other independent specific-heat measurement¹² of p -type Bi_2Te_3 , mentioned previously in connection with the lattice specific heat, gives a value of γ equal to $0.17 \pm 0.08 \text{ mJ g-at.}^{-1} \text{ deg}^{-2}$. This result is certainly incorrect, since it disagrees with the calculated γ well outside the combined limits of error. An additional reference,¹ cited earlier, finds no measurable electronic contribution, but neither the carrier type nor concentration is stated for the sample used.

D. Lattice Behavior

The substitution of selenium for tellurium significantly changes the lattice heat capacity and, as expected, raises the Debye temperature. At the lowest temperatures, Θ can be shown to vary as

$$\Theta_0 = K \bar{C}_1^{1/2} \Omega_0^{1/6} M^{-1/2}, \quad (17)$$

where Ω_0 is the atomic volume, M the molecular mass, K a constant, and \bar{C}_1 an average of the elastic constants. Since the rhombohedral angles of the unit cells given in Table IV for the two semiconductors are almost identical, $\Omega_0^{1/6}$ can be replaced in Eq. (17) by $a_0^{1/2}$ in computing the ratio of the limiting Debye temperature of Bi_2Se_3 to Bi_2Te_3 . This ratio is computed to be $1.08(\bar{C}_{\text{Bi}_2\text{Se}_3}/\bar{C}_{\text{Bi}_2\text{Te}_3})^{1/2}$. A comparison with the experimental value of 1.12 ± 0.04 indicates that the elastic constants of Bi_2Se_3 do not differ appreciably from those of Bi_2Te_3 .

While Θ_0^2 depends on the inverse of the mass $M_0 = 2M_1 + 3M_2$ with M_1 the gram atomic mass of bismuth

and M_2 of tellurium or selenium, the square of the high-temperature limiting Debye temperature Θ_∞^2 , is inversely proportional to a reduced mass, i.e.,

$$\Theta_\infty^2 \propto \frac{2}{M_1} + \frac{3}{M_2} \equiv \frac{1}{M_\infty}. \quad (18)$$

The ratios Θ_0/Θ_∞ and $(M_\infty/M_0)^{1/2}$ for both Bi_2Te_3 and Bi_2Se_3 are given in Table V. In the last column of this table is the product of $(\Theta_0/\Theta_\infty)(M_\infty/M_0)^{-1/2}$. These two numbers, which represent the constants of proportionality between Θ_0 and $M_0^{-1/2}$ and between Θ_∞ and $M_\infty^{-1/2}$, depend upon the interatomic forces in the crystal. They are approximately equal, thus suggesting that the interatomic forces are nearly the same for both semiconductors (in agreement with the approximate equality of the elastic constants stated above) and that the greater part in the change of Θ_0/Θ_∞ in going from Te to Se is due to the change in mass of one constituent.

VI. CONCLUSIONS

The specific heats of p -type and n -type bismuth telluride have been measured over the temperature range of 1.4–90°K. These measurements show that the lattice specific heats of the moderately doped n -type samples are essentially independent of the type and amount of dopant. For all carrier concentrations, the departure from the Debye T^3 approximation begins well below the lowest experimental points measured near 1.4°K. This behavior is the result of the highly

anisotropic nature of bismuth telluride, its compressed Brillouin zone and the existence of weak interlayer binding forces. The limiting Debye temperature Θ_0 found from these heat-capacity measurements is in good agreement with Θ_0 calculated from the elastic constants. Furthermore, the substitution of the lighter element selenium for tellurium raises the Debye temperature roughly in proportion to the square root of the ratio of the heavier to the lighter mass. This result implies similar elastic constants and interatomic forces for Bi_2Te_3 and Bi_2Se_3 .

The electronic specific heat of bismuth telluride has been shown to be dependent upon the type and number of carriers in the usual way but for n -type material with carrier concentrations exceeding $5 \times 10^{18} \text{ cm}^{-3}$, the electronic contribution can only be explained on the basis of the existence of an additional heavy-mass conduction band whose minimum lies approximately 30 meV above the minima of the lower six-ellipsoid conduction valleys. Such a heavy-mass band, postulated originally to explain the concentration dependence of the dHvA effect in Bi_2Te_3 , is therefore directly confirmed by these measurements.

ACKNOWLEDGMENTS

The authors gratefully acknowledge the help of T. Davis in calibrating the platinum resistance thermometer used in these experiments. Thanks are due also to H. Ashworth for making the Hall measurements on the samples, and to J. Jenkins for communicating the results of his elastic constant measurements.

Theory of Phonon-Assisted Optical Absorption in Semiconductors. I.

W. S. CHOW

Department of Physics, University of Cincinnati, Cincinnati, Ohio 45221

(Received 19 December 1968)

Green's-function techniques are applied to the investigation of phonon-assisted optical absorption in semiconductors. Different processes involved in phonon-assisted absorption are found, corresponding to different second-order diagrams in the expansion of the polarization function. Agreement is reached between the present theory and conventional perturbation theory. Some possible refinements are discussed.

I. INTRODUCTION

OPTICAL absorption by valence-band electrons in pure germanium for "direct" and "indirect" transitions to the conduction band has been calculated by Hall, Bardeen, and Blatt.¹ The direct transitions involve only the processes in which a valence-band electron absorbs a photon with momentum \mathbf{q} and

energy ω_0 to reach the conduction band. Because of the multivalley conduction-band structure of germanium, with consideration of only the direct transitions, the threshold absorption frequency should be larger than the energy gap between the two bands, which is defined as measured from the top of the valence band to the bottom of the valleys in the conduction band. The indirect phonon-assisted transitions are considered to take place through a virtual state which may be regarded as very short-lived. Energy is not conserved in

¹L. H. Hall, J. Bardeen, and F. J. Blatt, *Phys. Rev.* **95**, 559 (1954).